

GORDON W. GROVES  
 W. DALE BLAIR  
 Systems Research and  
 Technology Dept.  
 Naval Surface Warfare Center  
 Dahlgren Division  
 Dahlgren, VA 22448-5100  
 WINSTON C. CHOW  
 Warfare Analysis and Systems Dept.  
 Naval Surface Warfare Center  
 Dahlgren Division  
 Dahlgren, VA 22448-5100

## REFERENCES

- [1] Groves, G. W., and Blair, W. D. (1994)  
 Statistical studies of the monopulse ratio.  
 Technical Report TR-94/97, Naval Surface Warfare  
 Center Dahlgren Division, Dahlgren, VA, Oct. 1994.
- [2] Kanter, I. (1977)  
 The probability density function of the monopulse ratio  
 for  $N$  looks at a combination of constant and Rayleigh  
 targets.  
*IEEE Transactions on Information Theory*, IT-23, 5 (1977),  
 643-648.
- [3] Tullsson, B. (1991)  
 Monopulse tracking of Rayleigh targets: A simple  
 approach.  
*IEEE Transactions on Aerospace and Electronic Systems*,  
 27, 3 (July 1991), 520-531.
- [4] Seifer, A. D. (1992)  
 Monopulse-radar angle tracking in noise or noise  
 jamming.  
*IEEE Transactions on Aerospace and Electronic Systems*,  
 28, 3 (July 1992), 622-637.
- [5] Seifer, A. D. (1994)  
 Monopulse-radar angle measurement in noise.  
*IEEE Transactions on Aerospace and Electronic Systems*,  
 30, 3 (July 1994), 950-957.
- [6] Abramowitz, M., and Stegun, I. A. (1964)  
*Handbook of Mathematical Functions*.  
 New York: Dover, 1964.
- [7] Gradshteyn, I. S., and Ryzhik, I. M. (1980)  
*Table of Integrals, Series, and Products*.  
 New York: Academic Press, 1980, p. 1160.
- [8] Chow, W. C. (1996)  
 Analysis of the probability density function of the  
 monopulse ratio radar signal.  
 Technical report NSWCDD/TR-96/54, Naval Surface  
 Warfare Center, Dahlgren Division, Dahlgren, VA,  
 Aug. 1996.

## Upgrading Conical Scan With Off-Boresight Measurements

**Adding off-boresight measurements to a conical scan radar can bring the angle accuracy closer to the theoretical attainable limit. A model for off-boresight measurement implementation**

Manuscript received December 3, 1996; revised March 17, 1997.

IEEE Log No. T-AES/33/4/06857.

0018-9251/97/\$10.00 © 1997 IEEE

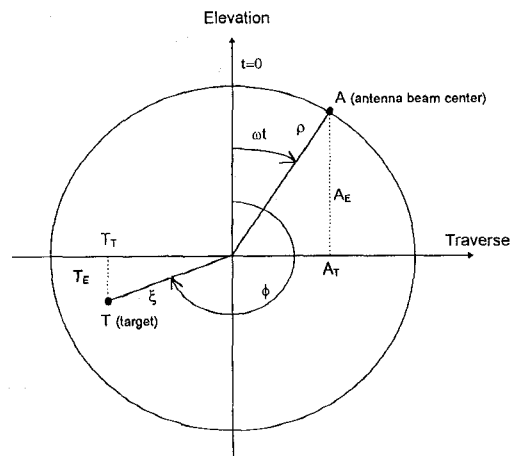


Fig. 1. Angular relationship between target and antenna.

and its performances are discussed. The expected accuracy is calculated and compared with the Cramer-Rao bound. The model is also used to determine bias error induced by the target dynamics.

## I. INTRODUCTION

Conical scan is a relatively simple angle tracking system. It presently finds use in noncombat applications like ranges, where a single and usually cooperative target (carrying a transponder or an emitter) is tracked.

Error analysis of off-boresight measurements in conical scan radar is discussed. Random error due to thermal noise or noise-like target fluctuations is considered. The system is modeled using ideal blocks and simplifying assumptions in order to simplify the analysis. The expected angle random error using the model is compared with the Cramer-Rao lower bound. Bias error due to target dynamics is also considered.

The analysis was prompted by an upgrade project of a conical scan radar. While the literature is abound with angle error analyses of monopulse radar [1-3], analyses of conical scan are rare [4].

## II. REVIEW OF CONICAL SCAN

Conical scan is an antenna tracking method in which an offset antenna beam is rotated around the boresight. The angle between the rotation axis (the boresight) and the axis of the antenna beam is called the squint angle. The echo from a target off boresight will be amplitude modulated with sinusoid-like signal at the rotation frequency. The amplitude of the echo signal modulation is relative to the angle between the boresight and the target line of sight. The phase of that modulation carries information on the angular direction of the target. Fig. 1 provides an angular view of the relative position of the antenna and the target in the traverse-elevation plane.

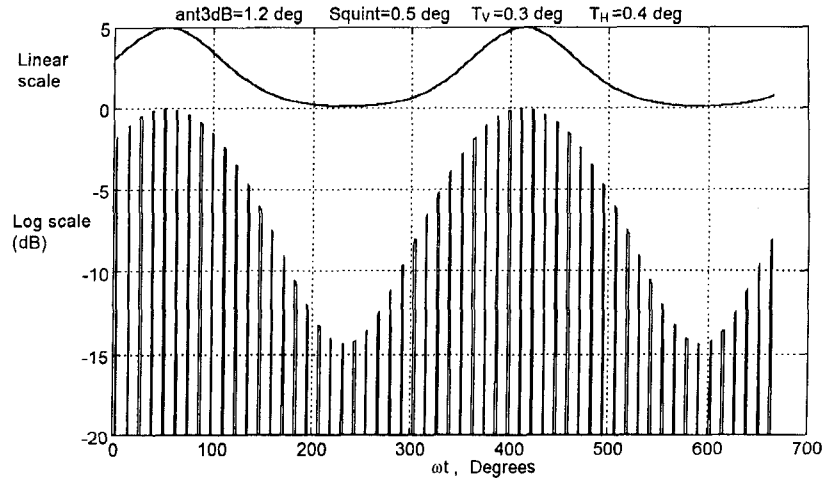


Fig. 2. Amplitude modulation by conical scan.

Note that all the parameters in Fig. 1 are angles.  $\rho$  is the squint angle of the antenna,  $\xi$  is the off-boresight angle of the target,  $\phi$  is the angle of the target error vector in the traverse-elevation plane, measured from the upward direction. The upward direction is selected as the antenna rotation angle  $\omega t$  at  $t = 0$ .  $\omega$  is the antenna rotation rate.

The elevation and traverse angles of the antenna  $A_E, A_T$ , and the target  $T_E, T_T$ , are given by

$$\begin{aligned} A_E(t) &= \rho \cos(\omega t), & A_T(t) &= \rho \sin(\omega t) \\ T_E &= \xi \cos(\phi), & T_T &= \xi \sin(\phi). \end{aligned} \quad (1)$$

The angle  $\theta(t)$  between the antenna beam axis and the target line of sight is given by

$$\cos \theta(t) \approx \frac{T_T A_T(t) + T_E A_E(t) + 1}{\sqrt{(\xi^2 + 1)(\rho^2 + 1)}}. \quad (2)$$

A typical antenna gain (power, one-way) is given by

$$G(\theta) = \left( \frac{\sin \left( 0.866\pi \frac{\theta}{\theta_{3 \text{ dB}}} \right)}{0.866\pi \frac{\theta}{\theta_{3 \text{ dB}}}} \right)^2. \quad (3)$$

Using  $\theta(t)$  from (2) in (3) yields the antenna gain as function of time for a given target direction. It is this rotation-induced gain variation that causes the amplitude modulation of the received target echo signal. Whether the antenna gain should be considered two-way or one-way depends on whether the target signal is due to skin reflection or to a transponder.

In our particular example we assume a linear relationship between the antenna power gain and the output of the envelope detector; Fig. 2 demonstrates the expected amplitude modulation for the case:

$$\rho = 0.5^\circ, \quad T_E = 0.3^\circ, \quad T_T = 0.4^\circ \quad \text{and} \quad \theta_{3 \text{ dB}} = 1.2^\circ.$$

Both linear scale and logarithmic scale are used in Fig. 2. Note that on the logarithmic scale the

modulation waveform resemblance to a sinusoid is more pronounced.

The purpose of the off-boresight measurement is to obtain the target line of sight direction defined by  $\xi$  and  $\phi$  (or by  $T_T$  and  $T_E$ ) from the depth (amplitude) and phase of the modulation waveform. We first assume that the target direction is fixed during the entire observation time.

### III. CRAMER-RAO LOWER BOUND FOR ESTIMATING $\xi$ AND $\phi$

To simplify the analysis we increase the pulsewidth until the pulse duration equals the pulse interval, while maintaining the average signal power. We can thus work with a continuous signal whose amplitude is modulated by the varying antenna gain. Assuming small off-boresight angle, the amplitude modulation is nearly sinusoidal, and the noise-free signal can be expressed as

$$s(t) = \text{Re}\{u(t) \exp(j\omega_c t)\}, \quad 0 \leq t \leq KT \quad (4)$$

where  $\omega_c$  is the carrier frequency and  $u(t)$  is the envelope

$$u(t) = A_0 [1 + m \cos(\omega t + \phi)] \quad (5)$$

and  $\omega$  is the antenna rotation frequency,  $T = 2\pi/\omega$ , and  $K$  is an integer. The signal  $s(t)$  is received with additive white Gaussian noise (AWGN) with two-sided power spectral density  $N_0/2$ . We are interested in the Cramer-Rao lower bound on the error in estimating  $m$  (which is related to the off-boresight angle  $\xi$ ) and  $\phi$ .

It can be shown that

$$\int_0^{KT} \frac{\partial u(t, m, \phi)}{\partial m} \frac{\partial u(t, m, \phi)}{\partial \phi} dt = 0 \quad (6)$$

which implies that the errors in  $m$  and  $\phi$  are independent.

Thus the Cramer–Rao lower bound [5] for the error in  $m$  is given by

$$\text{Var}\{m\} \geq \frac{N_0}{\int_0^{KT} \left( \frac{\partial u(t, m)}{\partial m} \right)^2 dt} \quad (7)$$

Using (5) in (7) yields

$$\text{Var}\{m\} \geq \frac{N_0}{\frac{A_0^2 KT}{2}} = \frac{N_0}{E} \quad (8)$$

where we have used the signal energy given by

$$E = \frac{A_0^2 KT}{2} \quad (9)$$

Note that  $\text{Var}\{m\}$  turned out to be a dimensionless signal-to-noise ratio, as befits a dimensionless  $m$ .

In order to convert the error in the modulation index  $m$  to an error in the off-boresight angle  $\xi$  we need the relationship between the two. We note from (5) that

$$m = \frac{A_{\max} - A_{\min}}{A_{\max} + A_{\min}} = \frac{G(\rho - \xi) - G(\rho + \xi)}{G(\rho - \xi) + G(\rho + \xi)} \quad (10)$$

For small  $\xi$  we can write

$$G(\rho + \xi) \approx G(\rho) + \xi \left. \frac{\partial G(\theta)}{\partial \theta} \right|_{\theta=\rho} \quad (11)$$

Using (11) in (10) yields

$$m(\xi) = -\frac{\xi}{G(\rho)} \left. \frac{\partial G(\theta)}{\partial \theta} \right|_{\theta=\rho} \quad (12)$$

Defining

$$k_\rho = \left( \frac{\xi}{m} \right)^2 = \left[ \frac{G(\rho)}{\left. \frac{\partial G(\theta)}{\partial \theta} \right|_{\theta=\rho}} \right]^2 \quad (13)$$

and using it in (8) we obtain

$$\text{Var}\{\xi\} \geq k_\rho \frac{N_0}{E} \quad (14)$$

Finally we should note that the signal energy is also a function of the squint angle. In one-way (transponder) operation

$$E = E_0 G(\rho) \quad (15)$$

In two-way radar, the dependence is on  $G^2(\rho)$ . Using (15) in (14) yields

$$\text{Var}\{\xi\} \geq \frac{k_\rho N_0}{G(\rho) E_0} = \frac{G(\rho)}{\left[ \left. \frac{\partial G(\theta)}{\partial \theta} \right|_{\theta=\rho} \right]^2} \frac{N_0}{E_0} \quad (16)$$

The Cramer–Rao bound for  $\phi$  is obtained from

$$\text{Var}\{\phi\} \geq \frac{N_0}{\int_0^{KT} \left( \frac{\partial u(t, \phi)}{\partial \phi} \right)^2 dt} \quad (17)$$

Using (5) and (9) in (17) yields

$$\text{Var}\{\phi\} \geq \frac{N_0}{\frac{m^2 A_0^2 KT}{2}} = \frac{N_0}{m^2 E} \quad (18)$$

Clearly the result in (18) makes sense intuitively. The smaller  $m$  is, the smaller will be the amplitude of the waveform whose phase we seek, hence the larger would be the expected error in estimating that phase. Obviously, very small  $m$  indicates very small off-boresight target direction  $\xi$ . In that case there is reduced importance to the angle  $\phi$ .

#### IV. FROM POLAR TO RECTANGULAR COORDINATES

So far we found the accuracy of the target angular position in polar coordinates  $\xi$  and  $\phi$ . We will now find the accuracy of the rectangular angles  $T_T$  and  $T_E$ . The two coordinate systems are related according to

$$T_T = \xi \sin \phi, \quad T_E = \xi \cos \phi. \quad (19)$$

Hence

$$\text{Var}\{T_T\} = \sin^2 \phi \text{Var}\{\xi\} + \xi^2 \cos^2 \phi \text{Var}\{\phi\} \quad (20)$$

$$\text{Var}\{T_E\} = \cos^2 \phi \text{Var}\{\xi\} + \xi^2 \sin^2 \phi \text{Var}\{\phi\}. \quad (21)$$

Using (13), (14) and (18) in (20) and (21) yields

$$\text{Var}\{T_T\} = \text{Var}\{T_E\} \geq k_\rho \frac{N_0}{E} \quad (22)$$

Equation (22) expresses the error variance as function of the signal energy  $E$ . The error variance will not change if we narrow the pulses and increase their amplitude, keeping the energy unchanged. We next assume a pulsed signal and a specific receiver implementation and obtain the error variance expected with that implementation.

#### V. RECEIVER MODEL

The circuitry model assumes a received signal from a Swerling II target, in a form of a train of RF pulses of width  $t_p$  and amplitude  $A_i$  (of the  $i$ th pulse). The signal amplitude contains a random component caused by two sources: 1) uncorrelated (from pulse to pulse) Rayleigh fluctuations of the target, and 2) thermal noise. Their combined effect is treated as an AWGN with two-sided power spectral density  $N_0/2$ . Assuming small off-boresight target direction, the pulse amplitude modulation, caused by the conical scan of the antenna, can be approximated by a sinusoidal waveform.

The receiver is described by the block diagram in Fig. 3. The signal is received by a matched filter, followed by an envelope detector and a logarithmic amplifier. The amplifier output is sampled once per pulse. From here on the processing is performed digitally. First the dc level is removed. Next, the

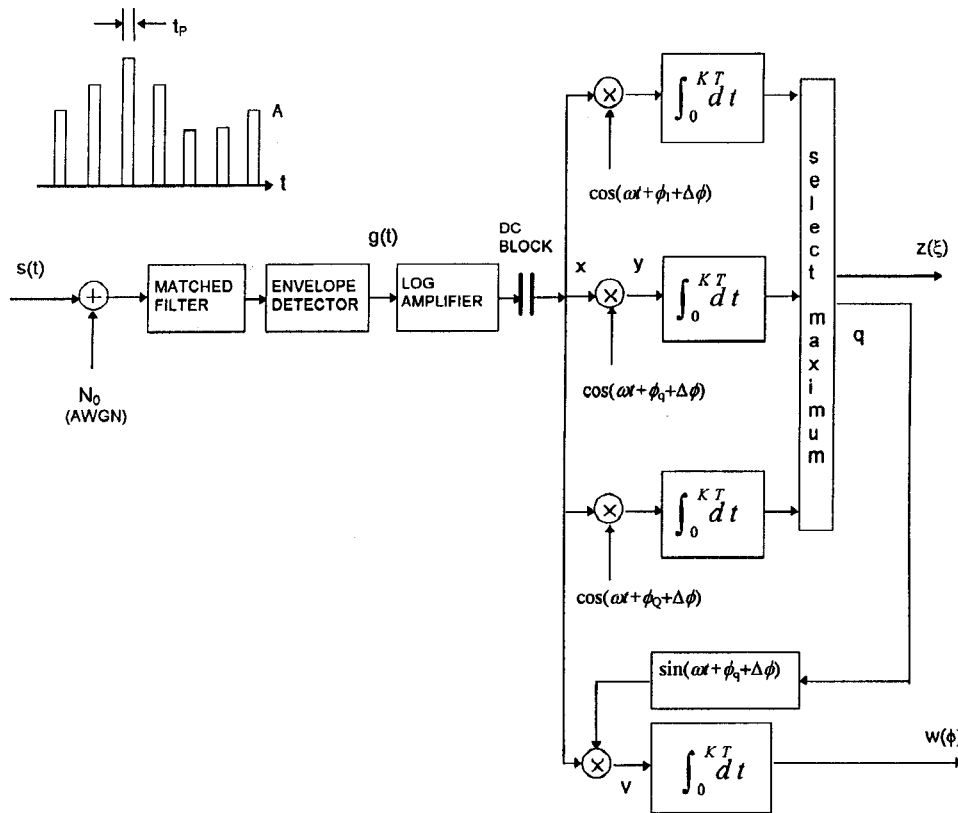


Fig. 3. Receiver implementation for estimating conical scan target parameters.

signal is processed in a bank of correlators. In each correlator the signal samples are multiplied by samples of a cosine signal at the antenna rotation frequency  $\omega$ . The reference signals to the different correlators differ in the phase shift, which corresponds to a different angle of the target from the initial angle of the scan. The integration in the correlators is performed over an integer number  $K$  of the scan period  $T$  ( $= 2\pi/\omega$ ). The correlator that yields the highest output identifies approximately the phase  $\phi$  and the corresponding output level  $z$  is proportional to the off-boresight angular distance  $\xi$ . We assume perfect calibration of a noise-free output level  $z$  as function of  $\xi$  and we are interested in the random error of that estimate of  $\xi$ .

The signal samples prior to the log amplifier could be approximated by samples of an amplitude modulated envelope with additive noise

$$g(t_i) = A_0 [1 + m(\xi) \cos(\omega t_i + \phi)] + n_i, \quad (23)$$

The critical parameter, which we try to estimate is the modulation index  $m(\xi)$ , because of its one-to-one relationship to the off-boresight angle  $\xi$ . The noise terms  $n_i$  are uncorrelated from sample to sample with a variance obtained from the Cramer-Rao bound on estimating the amplitude  $\hat{A}$  of a carrier pulse of duration  $t_p$ . This bound (see Appendix) is given by

$$\text{Var}\{n_i\} = \text{Var}\{\hat{A}\} = \frac{N_0}{t_p}. \quad (24)$$

The output of the log amplifier is

$$\log g(t_i) = \log A_0 + \log \left[ 1 + \frac{n_i}{A_0} + m \cos(\omega t_i + \phi) \right]. \quad (25)$$

The first term on the right-hand side (r.h.s.) is removed by the dc block. Assuming small off-boresight angular distance  $\xi < \theta_3$  dB, which causes  $m \ll 1$ , and assuming high signal-to-noise ratio, namely  $n_i \ll A_0$ , we can use the approximation

$$\log(1 + \varepsilon) \approx \varepsilon, \quad \varepsilon \ll 1 \quad (26)$$

and obtain the signal samples at the input to the bank of correlators

$$x(t_i) \approx \frac{n_i}{A_0} + m \cos(\omega t_i + \phi). \quad (27)$$

In the correlator whose phase is nearest the correct phase (the one with  $\phi_q = \phi$ ) the output of the synchronous multiplier is

$$\begin{aligned} y(t_i) &= x(t_i) \cos(\omega t_i + \phi + \Delta\phi) \\ &= \frac{m}{2} \cos(\Delta\phi) + \frac{n_i}{A_0} \cos(\omega t_i + \phi + \Delta\phi) \\ &\quad + \frac{m}{2} \cos(2\omega t_i + 2\phi + \Delta\phi) \end{aligned} \quad (28)$$

where  $\Delta\phi$  is the remaining phase difference. Assuming  $M$  pulses in each period  $T$  of the conical

scan, the samples are taken at times

$$t_i = i \frac{T}{M}. \quad (29)$$

Since the integration time is  $K$  scan periods, the integrator output is the sum

$$z = \sum_{i=0}^{KM-1} \left[ \frac{m}{2} \cos(\Delta\phi) + \frac{n_i}{A_0} \cos\left(\frac{2\pi i}{M} + \phi + \Delta\phi\right) + \frac{m}{2} \cos\left(\frac{2\pi i}{M} + 2\phi + \Delta\phi\right) \right]. \quad (30)$$

Because  $K$  is an integer, (30) reduces to

$$z = m \frac{KM}{2} \cos(\Delta\phi) + \sum_{i=0}^{KM-1} \frac{n_i}{A_0} \cos\left(\frac{2\pi i}{M} + \phi + \Delta\phi\right). \quad (31)$$

If the phase intervals between consecutive correlators is small,  $\Delta\phi$  must be small too, hence

$$\cos \Delta\phi \approx 1, \quad \Delta\phi \ll 1. \quad (32)$$

The expected value of  $z$  is therefore

$$\bar{z} = m \frac{KM}{2} \quad (33)$$

and its variance is

$$\text{Var}\{z\} = \frac{KM}{2} \text{Var}\left\{\frac{n_i}{A_0}\right\}. \quad (34)$$

Using (24) we get

$$\text{Var}\{z\} = \frac{KM}{2} \frac{N_0}{A_0^2 t_p}. \quad (35)$$

Setting the estimator of the modulation index  $m$  as

$$\hat{m} = \frac{2z}{KM} \quad (36)$$

we get

$$\bar{\hat{m}} = m, \quad (37)$$

$$\text{Var}\{\hat{m}\} = \frac{2N_0}{KMA_0^2 t_p}. \quad (38)$$

Note that the denominator of (38) is proportional to the energy in the  $KM$  pulses, since

$$E = \frac{1}{2} KMA_0^2 t_p. \quad (39)$$

Hence

$$\text{Var}\{\hat{m}\} = \frac{N_0}{E}. \quad (40)$$

The variance in (40) is identical to the Cramer–Rao bound (8).

Once  $z$  and the nearest phase reference  $\phi_q + \Delta\phi = \phi + \Delta\phi$  are found, it is necessary to find the exact phase, by estimating  $\Delta\phi$ . This can be implemented with one additional correlator that uses a *sine* reference. (To avoid sequential processing, a complete

additional set of correlators with *sine* references could be used and only the  $q$ th output selected.) The output of the multiplier in the *sine* correlator is

$$\begin{aligned} v(t_i) &= x(t_i) \sin(\omega t_i + \phi + \Delta\phi) \\ &= \frac{m}{2} \sin(\Delta\phi) + \frac{n_i}{A_0} \sin(\omega t_i + \phi + \Delta\phi) \\ &\quad + \frac{m}{2} \sin(2\omega t_i + 2\phi + \Delta\phi) \end{aligned} \quad (41)$$

and the output of the integrator

$$w = m \frac{KM}{2} \sin(\Delta\phi) + \sum_{i=0}^{KM-1} \frac{n_i}{A_0} \sin\left(\frac{2\pi i}{M} + \phi + \Delta\phi\right). \quad (42)$$

Similarly to the analysis for  $m$ , and using

$$\sin \Delta\phi \approx \Delta\phi, \quad \Delta\phi \ll 1 \quad (43)$$

we get for the correlator output  $w$

$$\text{Var}\{w\} = \frac{KM}{2} \text{Var}\left\{\frac{n_i}{A_0}\right\} = \frac{KM}{2} \frac{N_0}{A_0^2 t_p} \quad (44)$$

$$\bar{w} = m \frac{KM}{2} \Delta\phi. \quad (45)$$

Setting the estimator of  $m\Delta\phi$  as

$$m\Delta\hat{\phi} = \frac{2w}{KM} \quad (46)$$

will yield

$$\begin{aligned} \text{Var}(\hat{\phi}) &= \text{Var}(\Delta\hat{\phi}) \approx \left(\frac{2}{mKM}\right)^2 \text{Var}\{w\} \\ &= \frac{2N_0}{m^2 KMA_0^2 t_p} = \frac{1}{m^2} \frac{N_0}{E} \end{aligned} \quad (47)$$

which agrees with (18). We have thus demonstrated that, for the case of small off-boresight distance, high signal-to-noise ratio, and arbitrarily fine spacing between consecutive correlators, the receiver in Fig. 3 achieves the Cramer–Rao lower bound.

## VI. OPTIMAL SQUINT ANGLE

As pointed out in (13) the relationship between the “modulation index”  $m$  and the off-boresight angle  $\xi$  is defined by the antenna gain pattern (3), and by the squint angle  $\rho$ .

For the particular antenna gain pattern described in (3), (13) yields, for small  $\xi$ ,

$$\begin{aligned} k_\rho &= \left(\frac{\xi}{m}\right)^2 = \left[\frac{\rho}{2(1 - \alpha \cot \alpha)}\right]^2, \\ \alpha &= 0.866\pi \frac{\rho}{\theta_{3 \text{ dB}}}. \end{aligned} \quad (48)$$

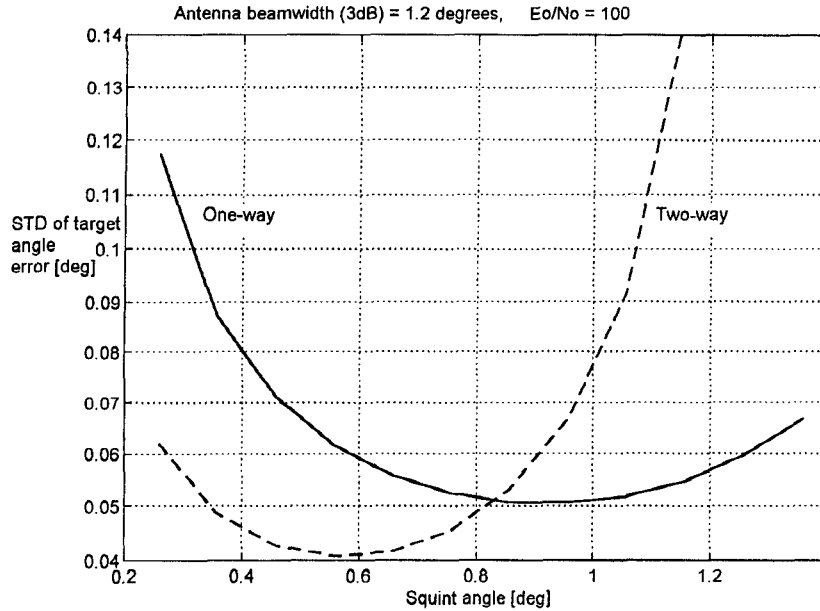


Fig. 4. Angle error STD versus squint angle.

Using (3), (15), and (48) in (22) we get for a one-way radar

$$\begin{aligned} \text{Var}\{T_T\} &= \text{Var}\{T_E\} \\ &\geq \left[ \frac{\rho}{2(1 - \alpha \cot \alpha)} \right]^2 \left( \frac{\alpha}{\sin \alpha} \right)^2 \frac{N_0}{E_0}; \end{aligned} \quad \text{One-way.} \quad (49)$$

For a two-way radar the antenna power gain pattern should be squared, yielding

$$\begin{aligned} \text{Var}\{T_T\} &= \text{Var}\{T_E\} \\ &\geq \left[ \frac{\rho}{4(1 - \alpha \cot \alpha)} \right]^2 \left( \frac{\alpha}{\sin \alpha} \right)^4 \frac{N_0}{E_0}; \end{aligned} \quad \text{Two-way.} \quad (50)$$

It is interesting to find out which squint angle  $\rho$  yields the smallest STD of the target angle error. The square root of (49) and (50) are plotted in Fig. 4, assuming  $\theta_{3 \text{ dB}} = 1.2^\circ$  and  $E_0/N_0 = 100$ . Fig. 4 shows that from the random error viewpoint, with the given antenna pattern, the optimal squint angle is approximately  $\frac{3}{4}\theta_{3 \text{ dB}}$  for one-way radar and  $\frac{1}{2}\theta_{3 \text{ dB}}$  for two-way radar.

Finally we should note that in practice the assumption of “sinusoidal modulation” with small index of modulation is not necessary, and calibration measurements will yield the necessary relationship between  $\xi$  and the correlator output  $z$ .

## VII. BIAS ERROR CAUSED BY TARGET DYNAMICS

Angle estimation using conical scan requires an extended measurement period—usually one or

more antenna rotation cycles. During that extended measurement period the direction difference between the antenna boresight and the target may change. Such a change could be caused by target dynamics, or by the antenna’s own servo control. Such a change in the relative direction of the target can cause a bias error in the estimated target angle.

The receiver model developed in Section V allows studying this bias error for different cases of target motion during the measurement period. Examples of the target angular trajectory and the resulting bias error are demonstrated in Figs. 5 and 6. In both figures the star represents the direction to the target at the center of the observation period, while the circle represents the noise-free estimated direction. In both cases the measurement period extends over 4 cycles of antenna rotations. Fig. 5 demonstrates that when the target track draws a straight line across the direction plane there is very little bias error due to the dynamics. When the target track has the shape of an arc or a spiral (Fig. 6), the direction is estimated at about 2/5 the way from the center of the arc to the center of arc’s chord. This last result repeated itself in many other arcs.

## VIII. CONCLUDING REMARKS

The theoretical bound on angle random error in conical scan was developed and a receiver was demonstrated, that achieves the bound (in small off-boresight error and high signal-to-noise ratio situation). However, well-known inherent limitations remain. Among them are: 1) operating with smaller than the maximum available signal energy due to the relatively lower antenna gain at the squint angle, 2) susceptibility to jamming, and 3) extended

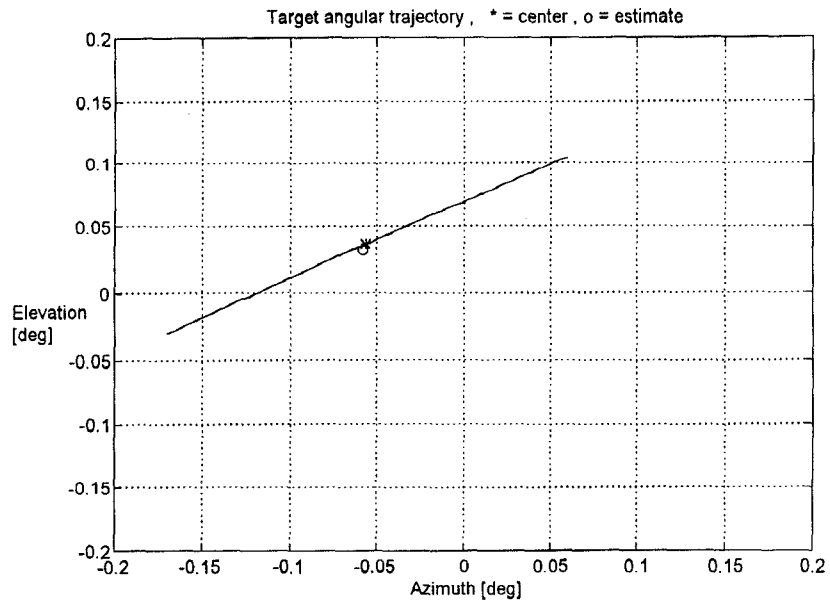


Fig. 5. Bias error caused by linear track of target in traverse-elevation plane.

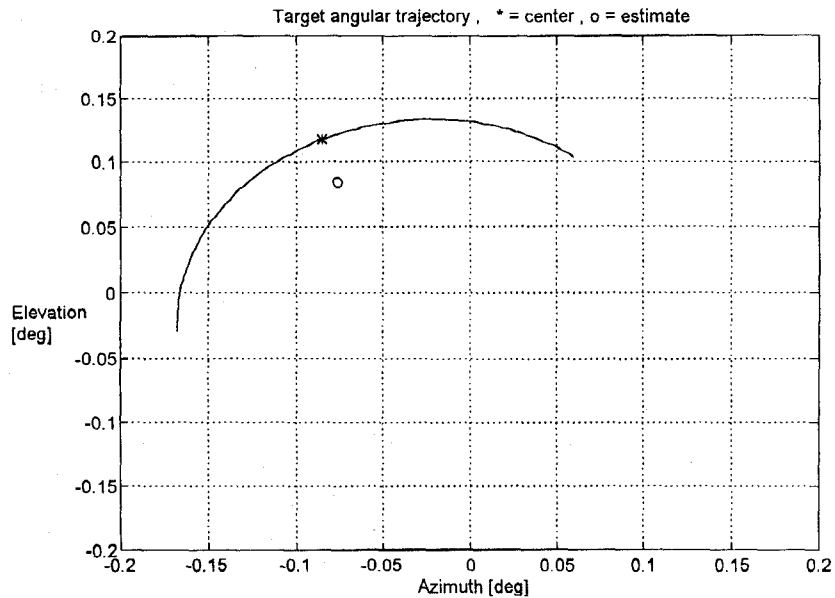


Fig. 6. Bias error caused by spiral track of target in traverse-elevation plane.

measurement period during which the direction to the target may change. Bias error caused by that last limitation was demonstrated for two typical cases.

#### APPENDIX. THE CRAMER-RAO BOUND OF CARRIER PULSE AMPLITUDE

Let the constant amplitude pulse be described by

$$s(t) = \text{Re}\{u(t) \exp(\omega_c t)\}, \quad -\frac{t_p}{2} \leq t \leq \frac{t_p}{2} \quad (51)$$

where  $\omega_c$  is the carrier frequency and  $u(t)$  is the envelope

$$u(t) = A. \quad (52)$$

The Cramer-Rao bound on the error in estimating  $\hat{A}$ , in the presence of AWGN with one-sided power spectral density  $N_0$ , is given by

$$\text{Var}\{\hat{A}\} \geq \frac{N_0}{\int_{-T_p/2}^{T_p/2} \left(\frac{\partial u}{\partial A}\right)^2 dt} = \frac{N_0}{t_p}. \quad (53)$$

NADAV LEVANON  
 Dept. of Electrical Engineering-Systems  
 Tel Aviv University  
 P.O. Box 39040, Ramat-Aviv  
 Tel Aviv, 69978  
 Israel

## REFERENCES

- [1] Sherman, S. M. (1984) *Monopulse Principles and Techniques*. Dedham, MA: Artech House, 1984.
- [2] Kanter, I. (1981) Varieties of average monopulse responses to multiple targets. *IEEE Transactions on Aerospace and Electronic Systems*, AES-17, 1 (Jan. 1981), 25–28.
- [3] Tullsson, B. E. (1991) Monopulse tracking of Rayleigh targets: A simple approach. *IEEE Transactions on Aerospace and Electronic Systems*, 27, 3 (May 1991), 520–531.
- [4] Barton, D. K., and Ward, H. R. (1969) *Handbook of Radar Measurements*. Englewood Cliffs, NJ: Prentice-Hall, 1969.
- [5] Van Trees, H. L. (1971) *Detection, Estimation, and Modulation Theory, Part I*. New York: Wiley, 1968, Sect. 4.2.3, pp. 273–287.

## An Efficient Decentralized Multiradar Multitarget Tracker for Air Surveillance

We present an efficient multiradar multitarget tracking (MTT) algorithm for air surveillance. This tracker uses a multisensor track-to-track correlation method called the sequential minimum normalized distance nearest neighbor (SMNDNN) correlation with the majority decision making MDM/OR logic to solve the multisensor assignment problem. A sequential fuser based on the mean square error criterion is then used to fuse the tracks generated by the trackers. Real-life multiradar data collected from an air surveillance radar network located along the coastline of Canada is used to evaluate the effectiveness of this distributed tracker. Analysis shows that this tracker provides a reliable air surveillance picture.

### I. INTRODUCTION

In order to make correct decisions, air defense and traffic control or, more generally, air command and control ( $C^2$ ) depend on a surveillance system to provide an overall picture of the air situation. To maintain an accurate and stable long range air picture, a surveillance system usually relies on a radar network to perform target tracking in an all-weather condition [1, 2]. There are three main architectures for a multiradar multitarget tracker:

Manuscript received July 31, 1995; revised March 5, 1996 and February 10, 1997.

IEEE Log No. T-AES/33/4/06858.

0018-9251/97/\$10.00 © 1997 IEEE

CORRESPONDENCE

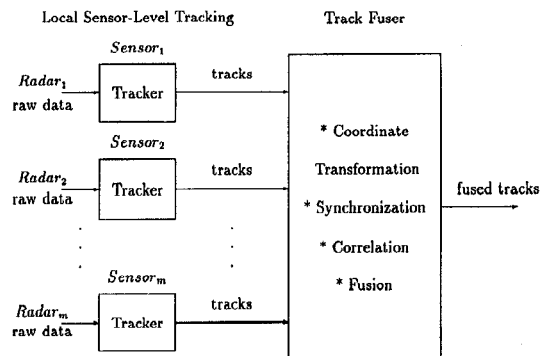


Fig. 1. Block diagram of distributed multiradar MTT system.

centralized [3], decentralized or hierarchical [4], and fully decentralized tracking [5, 6]. A decentralized tracker is of particular interest since it is more robust in the sense that center failure is less fatal to the whole surveillance system and the local sensors can retain their local tracking records. In addition, the decentralized approach is less costly since only one way narrowband communication channel is required.

An efficient decentralized multitarget tracking (MTT) architecture for real-life air surveillance is presented here. The decentralized tracker consists of two main components (Fig. 1): sensor-level tracking and multiradar track correlation and fusion. The first component generates the complete local track files to be processed by the fusion center. Here, we use a MTT tracker composed of the logic-based track initiation [7], the nearest neighbor (NN) data association [8], and a two-dimensional Kalman filter. The NN association is employed because our previous study based on real data shows marginal difference among the NN method and other data association techniques such as the joint probabilistic data association (JPDA) method [9]. The second component of the decentralized tracker combines the local track records to produce a more accurate and reliable coverage of the surveillance area. To do that, local track files have to be synchronized, correlated, and fused. The proposed tracker uses the sequential minimum normalized distance nearest neighbor (SMNDNN) method with the majority decision making (MDM/OR) logic for track correlation and the sequential minimum mean square error (MMSE) technique for track fusion. The main objective of this work is to investigate the effectiveness of this decentralized tracker in a real air surveillance environment. In Section II, we present the proposed decentralized multitarget tracker. In Section III, the radar network is briefly described. The performance of this proposed decentralized tracker is then evaluated using the real multiradar data. It is demonstrated that this decentralized tracking system provides an accurate air picture, even for maneuvering targets in a heavy clutter environment.